ANZIAM J. 56(2014), 116–137
doi:10.1017/S1446181114000339

A COMBINED FIRST-ORDER AND SECOND-ORDER VARIATION APPROACH FOR MULTIPLICATIVE NOISE REMOVAL

LE JIANG[1,2], JIN HUANG[2], JUN LIU[2] and XIAO-GUANG LV[✉1]

(Received 22 September, 2013; revised 4 April, 2014; first published online 22 December 2014)

Abstract

Denoising of images corrupted by multiplicative noise is an important task in various applications, such as laser imaging, synthetic aperture radar and ultrasound imaging. We propose a combined first-order and second-order variational model for removal of multiplicative noise. Our model substantially reduces the staircase effects while preserving edges in the restored images, since it combines advantages of the first-order and second-order total variation. The issues of existence and uniqueness of a minimizer for this variational model are analysed. Moreover, a gradient descent method is employed to solve the associated Euler–Lagrange equation, and several numerical experiments are given to show the efficiency of our model. In particular, a comparison with an existing model in terms of peak signal-to-noise ratio and structural similarity index is provided.

2010 *Mathematics subject classification*: 68U10.

Keywords and phrases: multiplicative noise removal, denoising, total variation, Euler–Lagrange equation, structural similarity index.

1. Introduction

Image denoising is a fundamental problem of interest to the mathematical community, and has wide applications in fields ranging from computer vision to medical imaging. The goal of image denoising is to reconstruct an approximation of an ideal image from an observed image. Over the past few decades, most of the literature has dealt with the additive noise. Given a noisy image $g = u + v$, where u and v represent

[1]School of Science, Huaihai Institute of Technology, Lianyungang, Jiangsu, 222005, China; e-mail: math_jiangle@126.com, xiaoguanglv@126.com.
[2]School of Mathematical Sciences/Institute of Computational Science, University of Electronic Science and Technology of China, Chengdu, Sichuan, 611731, China; e-mail: huangjin2345@126.com, sino.roy@163.com.

the original image and the noise, respectively, the denoising problem involving the additive noise is to recover u from the observed image g. Many approaches, such as traditional filtering, wavelets, stochastic approaches and variational methods have been proposed for solving the additive noise removal problem. We refer the reader to the articles [3, 4, 6, 9, 18, 36] for a review of image denoising algorithms.

However, multiplicative noise (also known as *speckled noise*) is quite different from additive noise, and is image dependent. Usually, it appears in laser imaging, synthetic aperture radar, ultrasound imaging and so on [16, 19, 39, 40]. In this paper, we deal with the multiplicative noise removal problem. For a mathematical description of such degradations, suppose that an original image, $u : \Omega \to \mathbb{R}$, is a real function defined on Ω, a connected bounded open subset of $\mathbb{R}^2$ with compact Lipschitz boundary. The goal of multiplicative noise removal is to recover the image u from the observed data

$$g = uv.$$

In this work, we concentrate on the assumption that v follows a gamma distribution, which commonly occurs in synthetic aperture radar (SAR). SAR images are strongly corrupted by speckle noise. A radar sends a coherent wave, which is reflected on the ground and then registered by the radar sensor. If the coherent wave is reflected on a coarse surface, then the image processed by the radar is degraded by a noise with large amplitude: this gives a speckled aspect to the image, and this is the reason why such noise is called speckle [17, 32]. In general, the multiplicative noise v of SAR images follows the gamma distribution with the probability density function [2]

$$P_V(v; L, M) = \frac{M^L v^{L-1}}{\Gamma(L)} e^{-Mv} \quad \text{for } v \geq 0, \tag{1.1}$$

where $\Gamma(\cdot)$ is the usual gamma function, and parameters L and M denote the inverse scale and shape parameters in the gamma distribution, respectively. Note that the mean of a gamma-distributed variable is L/M, and its variance is L/M^2. We assume that the mean of v equals one, which implies that $L = M$.

It is known that due to the coherent nature of these image acquisition processes, nearly all the information of the original image may vanish when it is distorted by the multiplicative noise. Multiplicative noise is one of the very complex noise models, which is also signal independent, non-Gaussian, and spatially dependent. Hence, its removal is a very challenging problem compared to the removal of additive Gaussian noise. Therefore, it is necessary to devise efficient and reliable algorithms for recovering the true images from the observed multiplicative noisy images. Early in the literature, a variety of methods were proposed to remove the multiplicative noise, such as geometric filter, adaptive filter [12, 42] and anisotropic diffusion methods [22, 43]. Recently, several variational models have been proposed to handle this problem. These methods have the ability to preserve edges very well in the denoised images. The first variational approach for multiplicative noise removal is the one by Rudin et al. [35] (commonly referred to as the RLO model). According to the statistical properties of the multiplicative noise v, the recovery of the image u is based on solving the

https://doi.org/10.1017/S1446181114000339 Published online by Cambridge University Press

constrained optimization problem

$$\min_u \int_\Omega |\nabla u|\, dx\, dy$$
$$\text{subject to} \quad \int_\Omega \frac{g}{u}\, dx\, dy = 1,$$
$$\text{and} \quad \int_\Omega \left(\frac{g}{u} - 1\right)^2 dx\, dy = \sigma^2.$$

The two constraints state that the mean of the noise is one, and the variance σ^2. Only basic statistical properties, such as the mean and the variance of the noise, v, are considered, so the method can not get a satisfactory restored result.

Aubert and Aujol [2] proposed a model (referred to as the AA model), whose minimizer corresponds to the denoised image to be recovered by using a *maximum a posteriori* (MAP) estimator. The AA model is a very famous model for the multiplicative noise removal problem, which utilizes total variation regularization due to its capability to preserve edges. This model is an unconstrained optimization problem which can be described as

$$\min_u \int_\Omega \log\left(u + \frac{g}{u}\right) dx\, dy + \lambda \int_\Omega |\nabla u|\, dx\, dy, \tag{1.2}$$

where the total variation of u is utilized as the regularization term, and λ is the regularization parameter, which controls the trade-off between a good fit of g and a smoothness requirement due to the total variation regularization. Although their proposed model is not convex, they still prove the existence of a minimizer and show the capability of their model through some numerical examples.

A drawback of the objective function (1.2) is that it is not convex for all u, so the solution obtained is most likely not the global optimal solution of (1.2). More recently, many convex models related to the AA model have been proposed. Shi and Osher [37] used the logarithmic transformation, and converted the multiplicative problem into an additive one. Then they added a quadratic term in the data term of the AA model and replaced the regularizer, TV(u) by TV($\log u$), where $\mathrm{TV}(u) = \int_\Omega |\nabla u|\, dx\, dy$. Hence, they derived a strictly convex TV minimization model (SO model) by setting $w = \log u$, and then applied a corresponding relaxed inverse scale space flow to solve the transformed problem. The same idea as the SO model was proposed by Huang et al. [20]; the authors modified the AA model by using an auxiliary variable $z = \log u$, then they solved the corresponding unconstrained model by a simpler alternating minimization algorithm. Bioucas-Dias and Figueiredo [5] proposed an efficient multiplicative noise removal method by using variable splitting and constrained optimization. They used variable splitting to obtain an equivalent constrained problem, and then solved this optimization problem by using the augmented Lagrangian method. A set of experiments verified that the proposed method, which they named MIDAL (multiplicative image denoising by augmented Lagrangian), yields state-of-the-art results in terms of both speed and denoising performance. Note that the regularization

https://doi.org/10.1017/S1446181114000339 Published online by Cambridge University Press

parameter, λ in (1.2), is an important quantity which controls the properties of the regularized solution, and λ should therefore be chosen with care. Recently, many methods involving the TV norm have been proposed, involving spatially adapted regularization parameters [10, 25].

Although the total variation regularization can realize significantly sharper edges and overall more visually pleasing images, it also tends to create piecewise-constant images even in regions with smooth transitions of grey values in the original image [8, 27]. This undesirable artefact is usually called the *staircase effect*. To alleviate staircase effects, second-order regularization schemes have been considered in the literature. There are two classes of second-order regularization methods for image restoration problems. The first class employs a second-order regularizer in a stand-alone way. For example, Chen et al. and Steidil [11, 38] considered a fourth-order partial differential equation (PDE) model for noise removal, and employed the dual algorithm of Chambolle [7] for solving the high-order problems. The high-order PDEs are known to behave much better than TV from the point of view of recovering smoother surfaces; however, they may not preserve edges very well. The second class combines the TV norm with a second-order regularizer. For example, Papafitsoros and Schönlieb [33] considered a high-order model involving convex functions of the first-order and second-order TV for image restoration problems. They used the split Bregman method [15] to numerically solve the corresponding discretized problem. A technique combining the TV filter with a fourth-order PDE filter was proposed to preserve edges and avoid staircase effects in smooth regions for noise removal [26, 28].

In order to avoid block effects (staircase effects) while achieving good trade-off between noise removal and edge preservation for the multiplicative noise removal problem, it is natural to utilize a combined first-order and second-order total variation technique. In this paper, we modify the AA model by adding a high-order functional into the energy. The proposed model can substantially reduce staircase effects, while preserving edges in the restored images, since it combines advantages of the first-order and second-order total variation. We study the issues of existence and uniqueness of a minimizer for this variational model. Moreover, we employ a gradient descent method to solve the associated Euler–Lagrange equation. Several numerical experiments are given to show the performance of our model. In particular, a comparison with AA model in terms of the peak signal-to-noise ratio and structural similarity index is provided as well.

The main contribution of this paper is twofold:

(i) We propose a hybrid total variational minimization model to solve the multiplicative noise removal problem. Since the proposed model combines the advantages of the TV regularization and the high-order TV model, it is able to avoid the blocky effects widely seen in images processed by TV regularization, while achieving a higher degree of noise removal and edge preservation.

(ii) The issues of existence and uniqueness of a minimizer for the proposed variational model are studied. Moreover, we employ a gradient descent method

https://doi.org/10.1017/S1446181114000339 Published online by Cambridge University Press

to solve the associated Euler–Lagrange equation. The numerical results show that our model avoids the creation of undesirable artefacts and blocky structures in the restored images which is a disadvantage of the TV regularization.

The rest of the paper is organized as follows. In the next section, we present the combined first-order and second-order total variational minimization for multiplicative noise removal, and carry out the mathematical analysis of the proposed model. In Section 3 we develop a gradient descent method to solve the associated Euler–Lagrange equation and give the details of its implementation. In Section 4 several numerical experiments are given to show the efficiency of the proposed method compared with the AA model. Some concluding remarks are given in Section 5.

2. The proposed model and mathematical analysis

We propose a new objective function for restoring images distorted by multiplicative noise. It is important that we apply a high-order total variation to the objective function for preserving edges and reducing the staircase effects in the restored images efficiently. We introduce our multiplicative denoising model from the statistical perspective, using the *Bayesian formulation* [24].

Let g, u, and v denote samples of instances of some random variables G, U and V, respectively. We assume that the random variable v is mutually independent and identically distributed on each pixel. Moreover, the random variable v in each pixel follows a gamma distribution (1.1) with $L = M$.

According to the posteriori estimation, the restored image u can be determined by

$$u = \underset{u}{\operatorname{argmax}}\, P_{U|G}(u|g). \tag{2.1}$$

From the Bayes rule, we have

$$P_{U|G}(u|g) = \frac{P_{G|U}(g|u)P_U(u)}{P_G(g)},$$

which implies

$$u = \underset{u}{\operatorname{argmax}}\, \frac{P_{G|U}(g|u)P_U(u)}{P_G(g)}.$$

Then, using a proposition of Aubert and Aujol [2], which yields $P_V(g/u)(1/u) = P_{G|U}(g|u)$, we obtain

$$P_{G|U}(g|u) = \frac{L^L g^{L-1}}{u^L \Gamma(L)} e^{-Lg/u}.$$

Taking the logarithmic transformation into account, we note that maximizing $P_{U|G}(u|g)$ amounts to minimizing

$$-\log(P_{U|G}(u|g)) = -\log(P_{G|U}(g|u)) - \log(P_U(u)) + \log(P_G(g)).$$

Since $P_G(g)$ is a constant, equation (2.1) can be rewritten as

$$u = \underset{u}{\operatorname{argmin}}[-\log\{P_{G|U}(g|u)\} - \log\{P_U(u)\}].$$

https://doi.org/10.1017/S1446181114000339 Published online by Cambridge University Press

It is clear that $-\log P_U(u)$ corresponds to the regularization term in the classical penalized likelihood approach to regularization [23]. However, in the Bayesian setting, $P_U(u)$ is the probability density, known as the *prior*, from which the unknown u is assumed to arise. Thus the prior knowledge regarding the characteristics of u can be formulated in the form of a probability density $P_U(u)$, and this yields a natural and statistically rigorous motivation for the regularization method.

Standard Tikhonov regularization corresponds to the following choice of the prior [1]:

$$P_U(u) = \exp^{-\lambda\|u\|_2^2/2}.$$

This corresponds to the assumption that the prior for u is a zero-mean Gaussian random variable with covariance matrix $\lambda^{-1}I$, which has the effect of penalizing reconstructions with large L_2-norm. For the L_2-norm of the gradient regularization, the penalty has a similar form, that is,

$$P_U(u) = \exp^{-\lambda\|\nabla u\|_2^2/2},$$

where ∇ is the gradient operator. The use of this regularization function has the effect of penalizing reconstructions that are not smooth. As an alternative to Tikhonov regularization, including standard Tikhonov regularization and gradient regularization for image noise removal, total variation regularization is another regularization technique that allows for the presence of sharp edges in the resulting reconstruction. In the case of total variational regularization, we have

$$P_U(u) = \exp^{-\lambda\|\nabla u\|_1},$$

where $\|\nabla u\|_1 = \int_\Omega |\nabla u|\,dx\,dy$ with $|\nabla u| = \sqrt{u_x^2 + u_y^2}$.

To reduce the staircase effects in the TV regularization, we consider a combined first-order and second-order variational model to restore blurred images corrupted by speckle noise in this work. In the proposed model, we assume that the prior probability density is of the form

$$P_u(u) = \exp^{-\gamma(\theta\|\nabla u\|_1 + (1-\theta)\|\nabla^2 u\|_1)},$$

where $\|\nabla^2 u\|_1 = \int_\Omega |\nabla^2 u|\,dx\,dy$ with $|\nabla^2 u| = \sqrt{u_{xx}^2 + u_{xy}^2 + u_{yx}^2 + u_{yy}^2}$, and θ is a weighting function that can be found adaptively. These considerations lead us to present the following functional for restoring images corrupted with multiplicative gamma noise:

$$\min_u E(u) = \int_\Omega \theta|\nabla u| + (1-\theta)|\nabla^2 u| + \lambda\left(\log u + \frac{g}{u}\right)dx\,dy, \tag{2.2}$$

where $\lambda = L/\gamma$ acts as a regularization parameter which measures the trade-off between the fidelity term $\int_\Omega (\log u + g/u)\,dx\,dy$ and a regularized term, and the parameter $\theta \in [0,1]$ is used to control the balance between the edges and the smooth surface.

Next, we recall the definitions of $BV(\Omega)$ and $BV^2(\Omega)$ [26, 28].

https://doi.org/10.1017/S1446181114000339 Published online by Cambridge University Press

DEFINITION 2.1. Let $\Omega \subset \mathbb{R}^N$ be an open subset with Lipschitz boundary. Define $BV(\Omega)$ as the subspace of the function $u \in L^1(\Omega)$ such that

$$\int_\Omega |Du| = \sup\Big\{\int_\Omega u \operatorname{div}(\varphi)\, dz \mid \varphi \in C_c^1(\Omega, R^N), |\varphi| \le 1\Big\},$$

called the BV seminorm, is finite. With respect to the norm $\|u\|_{BV(\Omega)} = \int_\Omega |Du| + \|u\|_{L^1(\Omega)}$, $BV(\Omega)$ is a Banach space.

DEFINITION 2.2. Let $\Omega \subset \mathbb{R}^N$ be an open subset with Lipschitz boundary. Define $BV^2(\Omega)$ as the subspace of the function $u \in L^1(\Omega)$ such that

$$\int_\Omega |D^2 u| = \sup\Big\{\int_\Omega \sum_{h,k=1}^{N} u\partial_k\partial_h\varphi^{hk}\, dz \mid \varphi \in C_c^2(\Omega, R^{N\times N}), |\varphi| \le 1\Big\}$$

with $|\varphi(x)| = \sqrt{\sum_{h,k=1}^{N}(\varphi^{hk})^2}$, called the BV^2 seminorm, is finite.

The functional $E(u)$ in (2.2) is defined on the set $BV(\Omega) \bigcap BV^2(\Omega)$; in particular, u must be positive almost everywhere in some cases. Some basic notation and properties of the spaces BV and BV^2 can be found in the articles by Li et al. [26] and Lysaker and Tai [28]. In this work, if a function g belongs to $L_\infty(\Omega)$, we denote by $\sup_\Omega g$ (respectively, $\inf_\Omega g$) the *essential supremum* of g (respectively, the *essential infimum* of g). We recall that the essential supremum $g = \inf\{C \in \mathbb{R} \mid g(z) \le C \text{ almost everywhere}\}$ and essential infimum $g = \sup\{C \in \mathbb{R} \mid g(z) \ge C \text{ almost everywhere}\}$. Motivated by the work of Aubert and Aujol [2], we have the following existence and uniqueness of the minimizer for the model (2.2).

THEOREM 2.3. *Let g be in $L_\infty(\Omega)$ with $\inf_\Omega g > 0$. Then the minimization problem (2.2) has at least one minimizer u^* in $BV(\Omega) \cap BV^2(\Omega)$, and u^* satisfies $0 < \inf_\Omega g \le u^* \le \sup_\Omega g$.*

PROOF. The proof is similar to that of [2, Theorem 4.3], and will be given in the Appendix for completeness. □

THEOREM 2.4. *Let $g > 0$ be in $L_\infty(\Omega)$. Then problem (2.2) has a unique solution $\hat{u}$ such that $0 < \hat{u} < 2g$.*

PROOF. Let u_1 and u_2 be two images defined on support Ω with $u_1 \ne u_2$. Then by Minkowski's inequality [31], we have

$$|\nabla(\tau u_1 + (1-\omega)u_2)| \le \omega|\nabla u_1| + (1-\omega)|\nabla u_2|$$

and

$$|\nabla^2(\omega u_1 + (1-\omega)u_2)| \le \omega|\nabla^2 u_1| + (1-\omega)|\nabla^2 u_2|$$

for each ω. Hence, $\theta|\nabla u| + (1-\theta)|\nabla^2 u|$ is convex. Let $f(u) = \log u + g/u$. Then $f'(u) = (u-g)/u^2$ and $f''(u) = (2g-u)/u^3$. If $0 < u < 2g$, then $f(u)$ is strictly convex. Therefore, the objective function $E(u)$ is strictly convex for $0 < u < 2g$, and it implies the uniqueness of a minimizer. This completes the proof. □

https://doi.org/10.1017/S1446181114000339 Published online by Cambridge University Press

3. Computational method

In this section, we derive the numerical method for problem (2.2) in detail. The directional derivative of $E(u)$ in (2.2) at u in the direction of v is given by

$$\begin{aligned}\frac{d}{d\epsilon}\bigg|_{\epsilon=0} E(u+\epsilon v) &= \frac{d}{d\epsilon}\bigg|_{\epsilon=0}\int_\Omega \bigg[\theta|\nabla(u+\epsilon v)| + (1-\theta)|\nabla^2(u+\epsilon v)| \\ &\quad + \lambda\bigg\{\log(u+\epsilon v) + \frac{g}{(u+\epsilon v)}\bigg\}\bigg]\,dx\,dy \\ &= \int_\Omega \frac{\theta(\nabla u\cdot\nabla v)}{|\nabla u|}\,dx\,dy + \int_\Omega \frac{(1-\theta)(\nabla u_x\cdot\nabla v_x + \nabla u_y\cdot\nabla v_y)}{|\nabla^2 u|}\,dx\,dy \\ &\quad + \lambda\int_\Omega \frac{u-g}{u^2}\,dx\,dy. \end{aligned} \tag{3.1}$$

Applying *Green's formula* [34] for the first term of (3.1), we have

$$\int_\Omega \frac{\theta(\nabla u\cdot\nabla v)}{|\nabla u|}\,dx\,dy = \int_{\partial\Omega}\frac{\theta}{|\nabla u|}\nabla u\cdot Nv\,dS - \int_\Omega \nabla\cdot\bigg(\frac{\theta\nabla u}{|\nabla u|}\bigg)v\,dx\,dy,$$

where $N=(n_1,n_2)$ is the unit outer normal vector of $\partial\Omega$. Using the same formula for the second term of (3.1), we get

$$\begin{aligned}&\int_\Omega \frac{(1-\theta)(\nabla u_x\cdot\nabla v_x + \nabla u_y\cdot\nabla v_y)}{|\nabla^2 u|}\,dx\,dy \\ &\quad= \int_\Omega \frac{(1-\theta)\nabla u_x}{|\nabla^2 u|}\cdot\nabla v_x\,dx\,dy + \int_\Omega \frac{(1-\theta)\nabla u_y}{|\nabla^2 u|}\cdot\nabla v_y\,dx\,dy \\ &\quad= \int_{\partial\Omega}\bigg[\frac{(1-\theta)\nabla u_x}{|\nabla^2 u|}\cdot Nv_x + \frac{(1-\theta)\nabla u_y}{|\nabla^2 u|}\cdot Nv_y\bigg]\,dS \\ &\qquad- \int_\Omega\bigg[\nabla\cdot\bigg(\frac{(1-\theta)\nabla u_x}{|\nabla^2 u|}\bigg)v_x + \nabla\cdot\bigg(\frac{(1-\theta)\nabla u_y}{|\nabla^2 u|}\bigg)v_y\bigg]\,dx\,dy.\end{aligned}$$

Let $W=(\nabla\cdot\{(1-\theta)\nabla u_x/|\nabla^2 u|\},\nabla\cdot((1-\theta)\nabla u_y/|\nabla^2 u|))$. Thus, applying Green's formula for the last term of the above equation, we have

$$\begin{aligned}&\int_\Omega\bigg[\nabla\cdot\bigg(\frac{(1-\theta)\nabla u_x}{|\nabla^2 u|}\bigg)v_x + \nabla\cdot\bigg(\frac{(1-\theta)\nabla u_y}{|\nabla^2 u|}\bigg)v_y\bigg]\,dx\,dy \\ &\quad= \int_\Omega W\cdot\nabla v\,dx\,dy \\ &\quad= \int_{\partial\Omega} W\cdot Nv\,dx\,dy - \int_\Omega \nabla\cdot Wv\,dx\,dy\end{aligned}$$

https://doi.org/10.1017/S1446181114000339 Published online by Cambridge University Press

$$= \int_{\partial\Omega}\left[\nabla.\left(\frac{(1-\theta)\nabla u_x}{|\nabla^2 u|}\right)n_1 v + \nabla\cdot\left(\frac{(1-\theta)\nabla u_y}{|\nabla^2 u|}\right)n_2 v\right]dS$$

$$- \int_{\Omega}\left[\left\{\nabla\cdot\left(\frac{(1-\theta)\nabla u_x}{|\nabla^2 u|}\right)\right\}_x v + \left\{\nabla\cdot\left(\frac{(1-\theta)\nabla u_y}{|\nabla^2 u|}\right)\right\}_y v\right]dx\,dy.$$

Therefore,

$$\begin{aligned}\frac{d}{d\epsilon}\Big|_{\epsilon=0} E(u+\epsilon v) &= \int_{\partial\Omega}\frac{\theta}{|\nabla u|}\nabla u\cdot N v\,dS - \int_{\Omega}\nabla\cdot\left(\frac{\theta\nabla u}{|\nabla u|}\right)v\,dx\,dy\\ &+ \int_{\partial\Omega}\left[\frac{(1-\theta)\nabla u_x}{|\nabla^2 u|}\cdot N v_x + \frac{(1-\theta)\nabla u_y}{|\nabla^2 u|}\cdot N v_y\right]dS\\ &- \int_{\partial\Omega}\left[\nabla\cdot\left(\frac{(1-\theta)\nabla u_x}{|\nabla^2 u|}\right)n_1 v + \nabla\cdot\left(\frac{(1-\theta)\nabla u_y}{|\nabla^2 u|}\right)n_2 v\right]dS\\ &+ \int_{\Omega}\left[\left\{\nabla\cdot\left(\frac{(1-\theta)\nabla u_x}{|\nabla^2 u|}\right)\right\}_x v + \left\{\nabla\cdot\left(\frac{(1-\theta)\nabla u_y}{|\nabla^2 u|}\right)\right\}_y v\right]dx\,dy\\ &+\lambda\int_{\Omega}\frac{u-g}{u^2}\,dx\,dy.\end{aligned}$$

We can easily obtain the associated *Euler–Lagrange equation* [14] under a fixed θ for (2.2):

$$0 = -\theta\,\nabla\cdot\left(\frac{\nabla u}{|\nabla u|}\right) + (1-\theta)\left[\left\{\nabla\cdot\left(\frac{\nabla u_x}{|\nabla^2 u|}\right)_x\right\} + \left\{\nabla\cdot\left(\frac{\nabla u_y}{|\nabla^2 u|}\right)_y\right\}\right] + \lambda\frac{u-g}{u^2}$$

with the boundary conditions

$$\nabla u\cdot N = 0,\quad \nabla u_x\cdot N = 0,\quad \nabla u_y\cdot N = 0,$$

$$\nabla\cdot\left(\frac{\nabla u_x}{|\nabla^2 u|}\right)n_1 = 0,\quad \nabla\cdot\left(\frac{\nabla u_y}{|\nabla^2 u|}\right)n_2 = 0,$$

where $N = (n_1, n_2)$ denotes the unit outer normal vector of $\partial\Omega$ [26, 28].

From the Euler–Lagrange variation principle [14], the minimizer of u can be interpreted as the steady-state solution of the associated heat flow:

$$\begin{aligned}\frac{\partial u}{\partial t} &= \theta\left[\left(\frac{u_x}{|\nabla u|}\right)_x + \left(\frac{u_y}{|\nabla u|}\right)_y\right] - (1-\theta)\left[\left(\frac{u_{xx}}{|\nabla^2 u|}\right)_{xx} + \left(\frac{u_{xy}}{|\nabla^2 u|}\right)_{yx} + \left(\frac{u_{yx}}{|\nabla^2 u|}\right)_{xy}\right.\\ &\left. + \left(\frac{u_{yy}}{|\nabla^2 u|}\right)_{yy}\right] - \lambda\frac{u-g}{u^2}.\end{aligned} \tag{3.2}$$

https://doi.org/10.1017/S1446181114000339 Published online by Cambridge University Press

We use the finite difference scheme to discretize (3.2) (see, for example, [26, 28] for more details). In the implementations, we use the following discretization with the step size $h = 1$.

$D_x^{\pm}u_{i,j}$	$\pm(u_{i\pm1,j} - u_{i,j})$
$D_y^{\pm}u_{i,j}$	$\pm(u_{i,j\pm1} - u_{i,j})$
$D_{xx}u_{i,j}$	$D_x^{+}u_{i,j} - D_x^{+}u_{i-1,j}$
$D_{xy}^{\pm}u_{i,j}$	$\pm[D_x^{\pm}u_{i,j\pm1} - D_x^{\pm}u_{i,j}]$
$D_{yx}^{\pm}u_{i,j}$	$\pm[D_y^{\pm}u_{i\pm1,j} - D_y^{\pm}(u_{i,j})]$
$D_{yy}u_{i,j}$	$D_y^{+}u_{i,j} - D_y^{+}u_{i,j-1}$
$\lvert D_x u_{i,j}\rvert$	$\sqrt{(D_x^{+}u_{i,j})^2 + (m[D_y^{+}u_{i,j}, D_y^{-}u_{i,j}])^2 + \delta}$
$\lvert D_y u_{i,j}\rvert$	$\sqrt{(m[D_x^{+}u_{i,j}, D_x^{-}u_{i,j}])^2 + (D_y^{+}u_{i,j})^2 + \delta}$
$\lvert D^2 u_{i,j}\rvert$	$\sqrt{(D_{xx}u_{i,j})^2 + (D_{xy}^{+}u_{i,j})^2 + (D_{yx}^{+}u_{i,j})^2 + (D_{yy}u_{i,j})^2 + \delta}$

In the discretization, we use the notation $m[a, b] = (\operatorname{sgn} a + \operatorname{sgn} b)/2 \cdot \min(|a|, |b|)$, and the small parameter $\delta > 0$ is introduced to avoid division by zero. The time step and space step are denoted by τ and h, respectively. Also, we denote the time and space coordinates as follows:

$$\begin{cases} t = n\tau & n = 0, 1, 2, \ldots, \\ x = ih & i = 0, 1, 2, \ldots, I, \\ y = jh & j = 0, 1, 2, \ldots, J, \end{cases}$$

where $Ih \times Jh$ is the size of the image support. We denote by u^k the approximation for $u(x, y, k, \tau)$ where x and y are the grid points. Finally, we get the following explicit computation scheme for (3.2):

$$\begin{aligned} u^{k+1} = u^k + \tau\theta\left[D_x^{-}\frac{D_x^{+}u^k}{|D_x u^k|} + D_y^{-}\frac{D_y^{+}u^k}{|D_y u^k|}\right] + \tau(1-\theta)\left[D_{xx}\left(\frac{D_{xx}u^k}{|D^2u^k|}\right) + D_{yx}^{-}\left(\frac{D_{xy}^{+}u^k}{|D^2u^k|}\right)\right. \\ \left. + D_{xy}^{+}\left(\frac{D_{yx}^{-}u^k}{|D^2u^k|}\right) + D_{yy}\left(\frac{D_{yy}u^k}{|D^2u^k|}\right)\right] - \tau\lambda\frac{u^k - g}{(u^k)^2 + \beta}, \end{aligned} \tag{3.3}$$

where the parameter β is introduced to avoid division by zero. There is an issue of choosing the optimal step size τ which ensures speedy convergence. Lysker and Tai [28] have shown that the numerical scheme is stable if equation (3.3) is solved as long as τ fulfils the Courant–Friedrichs–Lewy (CFL) stability criterion [28, 29]. Due to the severe nonlinearity of the equation, however, such an optimal step size is difficult to obtain theoretically, and is computationally very expensive. In numerical examples, we empirically choose a suitable value of τ that satisfies the CFL condition.

Next, we discuss the choice of the weighting parameter θ in equation (3.3). Due to the strengths and weaknesses of the first-order and second-order variation approach, it is desirable that the weighting parameter $\theta = 1$ along edges and in flat regions,

https://doi.org/10.1017/S1446181114000339 Published online by Cambridge University Press

emphasizing the restoration properties for the first-order total variation. To emphasize the restoration properties for the second-order total variation in smooth regions, we want $0 \le \theta < 1$. Specifically, the resulting algorithm for (3.3) is just the TV regularization method for then multiplicative noise removal problem when $\theta = 1$, while the resulting algorithm is the second-order TV regularization method when $\theta = 0$. Usually, we may compute the parameter θ by using the information of the edges and smooth regions of the resulting image obtained by smoothing the observed image g with low-pass filters such as the median filter and the Gauss filter. We have carried out some numerical experiments. In order to detect edges and smoothing regions much better, we adopt the method of Lysker and Tai [28] for updating θ. The results obtained from various numerical examples show that the updating procedure behaves better for our model than the fixed θ. This is because, as the iteration proceeds, the edges and smoothing regions of the recovered image are closer to the original image; thus the parameter θ computed by the updating scheme is more suitable for restoration. So we employ this method [28] for updating θ in our numerical experiments too. Suppose that u^k is the kth iterative solution. We update the parameter θ as follows:

$$\theta_{i,j} = \begin{cases} 1 & \text{if } \dfrac{|\nabla u^k_{i,j}|}{\max\limits_{i,j}(|\nabla u^k_{i,j}|)} \ge c, \\ \dfrac{1}{2}\cos\left(\dfrac{2\pi|\nabla u^k_{i,j}|}{c\max\limits_{i,j}(|\nabla u^k_{i,j}|)}\right) + \dfrac{1}{2} & \text{otherwise,} \end{cases} \tag{3.4}$$

where $0 \ll c < 1$, which implies that only the absolute largest jumps, the largest of $|\nabla u^k|$, are unaffected by the high-order regularization. As reported by Lysker and Tai [28], for large and small values of $|\nabla u^k|$, the parameter θ is closer to one, and for intermediate values of $|\nabla u^k|$, the parameter θ approaches zero, which means that the high-order filter dominates the computation, and the staircase effect is suppressed. Since only small jumps should be suppressed with the high-order regularization, it is useful to set $c = 1/8$.

We are now in a position to describe the *time-marching gradient descent algorithm* for restoring images corrupted by the multiplicative noise.

Algorithm 1: Time-marching gradient descent algorithm for solving (2.2)

Input : g, *MaxIter*, λ and τ and initialize u^0
Iteration: For $k = 1$:*MaxIter*
1 Compute u^k using the explicit scheme (3.3).
2 Update the parameter θ according to (3.4).
end.

Similarly, with the method of Aubert and Aujol [2], it is easy to modify our model to incorporate a linear blurring operator K. In this case, the minimization function (2.2) becomes

$$\min_u \left\{ E(u) = \int_\Omega \theta|\nabla u| + (1-\theta)|\nabla^2 u| + \lambda\left(\log Ku + \frac{g}{Ku}\right) dx \right\}. \tag{3.5}$$

https://doi.org/10.1017/S1446181114000339 Published online by Cambridge University Press

We use the following explicit computation scheme to obtain the minimizer for problem (3.5):

$$u^{k+1} = u^k + \tau(1-\theta)\left[D_x^- \frac{D_x^+ u^k}{|D_x u^k|} + D_y^- \frac{D_y^+ u^k}{|D_y u^k|}\right] + \tau\theta\left[D_{xx}\left(\frac{D_{xx}u^k}{|D^2 u^k|}\right) + D_{yx}^-\left(\frac{D_{xy}^+ u^k}{|D^2 u^k|}\right)\right]$$
$$+ \tau\theta\left[D_{xy}^+\left(\frac{D_{yx}^- u^k}{|D^2 u^k|}\right) + D_{yy}\left(\frac{D_{yy}u^k}{|D^2 u^k|}\right)\right] - \tau\lambda K^T \frac{Ku^k - g}{(Ku^k)^2 + \beta}. \tag{3.6}$$

Based on the computation scheme (3.6) and update formula (3.4), we obtain the following algorithm for restoring blurred images corrupted by multiplicative noise.

Algorithm 2: Time-marching gradient descent algorithm for solving (3.5)

Input : k, g, *MaxIter*, λ and τ and initialize u^0
Iteration: For k = 1:*MaxIter*
1 Compute u^k using explicit scheme (3.6).
2 Update the parameter θ according to (3.4).
end.

4. Numerical experiments

We present some numerical results to illustrate the performance of the proposed model for multiplicative noise removal. We compare our approach with the AA model of Aubert and Aujol [2]. Note that both the AA model and the proposed model are solved by the time-marching method. For convenience, we use the terms terminology "model" and "method" interchangeably in this work. All experiments were carried out in Windows XP and Matlab v7.10 running on a desktop equipped with an Intel Core2 Duo CPU 2.93 GHz and 3 GB of RAM. The initial guess is chosen to be the observed image in all tests.

The quality of the restoration results by the two different methods is compared quantitatively by using the relative error, the peak signal-to-noise ratio (PSNR) and structural similarity index (SSIM). PSNR is an engineering term for the ratio between the maximum possible power of a signal and the power of corrupting noise that affects the fidelity of its representation. In general, a high PSNR value indicates that the restoration is more accurate. The SSIM is a well-known quality metric, used to measure the similarity between two images. This method, developed by Wang et al. [41], is based on three specific statistical measures that are much closer to how the human eye perceives differences between two images.

Suppose u, g and $\tilde{u}$ are the original image, the noisy image and the restored image, respectively. The relative error of the restored image with respect to the original image is defined as

$$\text{RelErr} = \frac{\|u - \tilde{u}\|_2}{\|u\|_2}$$

https://doi.org/10.1017/S1446181114000339 Published online by Cambridge University Press

(a)  (b)  (c) 

FIGURE 1. Original images (256 × 256). (a) "Cameraman". (b) "Lena". (c) "House".

The PSNR is defined by

$$\mathrm{PSNR} = 10 \log \frac{n^2 \mathrm{Max}_I^2}{\|u - \tilde{u}\|_2^2},$$

where Max_I is the maximum possible pixel value of the image, and if the pixels are represented by using 8 bits per sample, it is usually 255. The SSIM is given by

$$\mathrm{SSIM} = \frac{(2\mu_u\mu_{\tilde{u}} + C_1)(2\sigma_{u\tilde{u}} + C_2)}{(\mu_u^2 + \mu_{\tilde{u}}^2 + C_1)(\sigma_u^2 + \sigma_{\tilde{u}}^2 + C_2)},$$

where μ_u and $\mu_{\tilde{u}}$ are averages of u and $\tilde{u}$, respectively; σ_u and $\sigma_{\tilde{u}}$ are the variance of u and $\tilde{u}$, respectively; $\sigma_{u\tilde{u}}$ is the covariance of u and $\tilde{u}$. The positive constants C_1 and C_2 can be thought of as stabilizing constants for near-zero denominator values. In the following experiments, we will also use an SSIM map to reveal areas of high or low similarity between two images. A whiter SSIM map indicates that the two images are closer. We refer the reader to the article by Wang et al. [41] for further details on SSIM and SSIM maps.

We use eight images to test the proposed method: four simulated images and four real SAR images, partly from http://www.sandia.gov/radar/complex_data. For the AA method and the proposed method, we use the time-marching algorithm to solve the corresponding Euler–Lagrange equations. We set the step size τ to 0.1 in order to obtain a stable iterative procedure. In the experiments, we adjust the parameter λ for the two methods to be optimal in the sense that after many trials, the parameter gives the best restoration. The algorithms are stopped when the maximum number of iterations is reached. For four real SAR images, since no corresponding reference image exists, and, since we cannot compare the AA method and the proposed method numerically, we just present the results obtained by the proposed method.

The first three original images are displayed in Figure 1. In the first test, we aim to restore the image "Cameraman" corrupted by multiplicative noise with $L = 15$ and $L = 5$, respectively. We show the restored results for $L = 15$ in Figure 2. It is clear from Figure 2 that the proposed method outperforms the AA method. The images recovered by the proposed method have much smoother background than those recovered by the AA method, and at the same time, the edges can be preserved as well. For better

https://doi.org/10.1017/S1446181114000339 Published online by Cambridge University Press

FIGURE 2. Results of different methods for removing multiplicative noise with $L = 15$ (Cameraman): (a) the noisy image corrupted by multiplicative noise; (b) the restored image by the AA method; (c) the restored image by the proposed method.

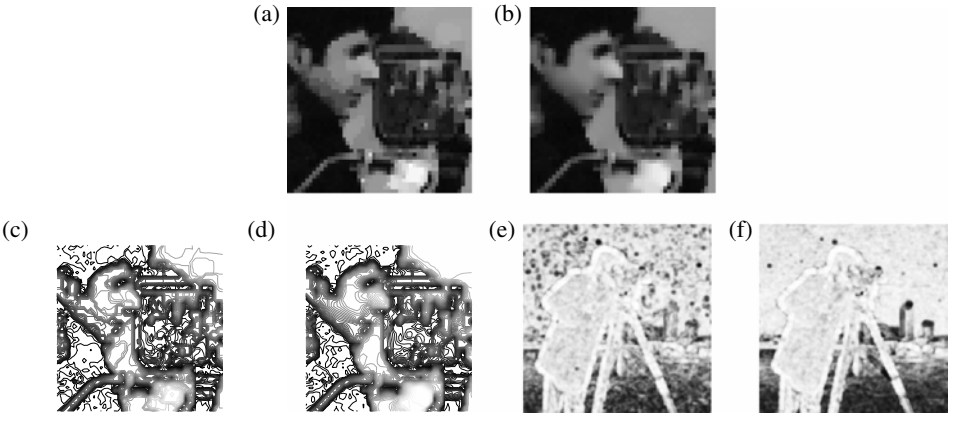

FIGURE 3. The small portions and the SSIM maps of the restored images with $L = 15$ (Cameraman). (a) and (b) are small parts of the restored images; (c) and (d) are contours of small parts; (e) and (f) are SSIM maps of the restored images.

visualization, we zoom in on small parts of the recovered images and display them in Figure 3. From the first row in Figure 3, the results obtained by the AA method have some piecewise constant regions, while our method can restore images with smoother surfaces. This effect is even better visualized in a contour plot in the second row, since we can see from the contour plots of the face and the trouser-legs of the cameraman that the contour plots obtained by the proposed method are significantly smoother at smooth regions than those obtained by the AA method. We also present the SSIM maps of the restored images in Figures 3(e)–(f). Note that the SSIM maps of the restored images by the proposed method are whiter than those by the AA method, that is, our method can get better restoration results.

In Figures 4 and 5, we compare the AA method with our method for recovering the noisy image "Lena" with $L = 10$. The zoomed-in parts of the reconstructed images for $L = 10$ and the SSIM maps are shown in Figure 5. From visual inspection of the

https://doi.org/10.1017/S1446181114000339 Published online by Cambridge University Press

FIGURE 4. Results of different methods for removing multiplicative noise with $L = 10$ (Lena): (a) the noisy image corrupted by multiplicative noise; (b) the restored image by the AA method; (c) the restored image by the proposed method.

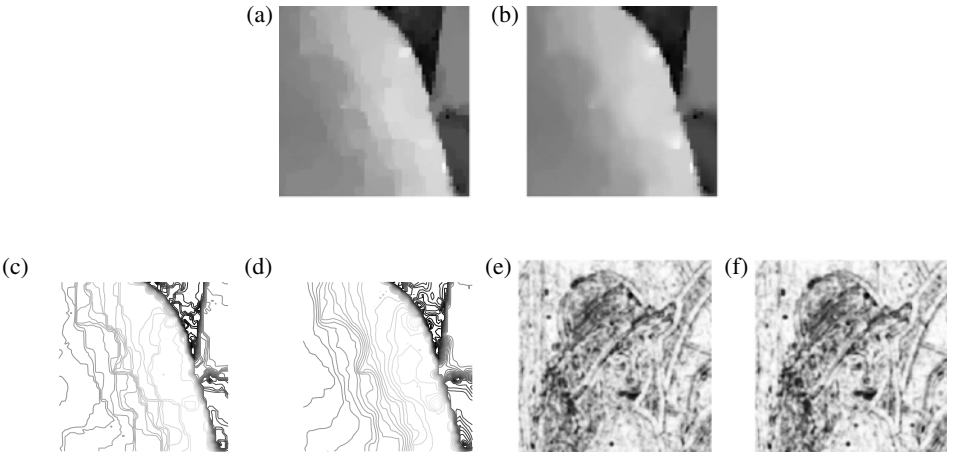

FIGURE 5. The small portions and the SSIM maps of the restored images with $L = 10$ (Lena): (a) and (b) are small parts of the restored images; (c) and (d) are contours of the small parts; (e) and (f) are SSIM maps of the restored images.

images it is evident that the face, nose and shoulder of "Lena" are much more smoothly obtained by our method than by the AA method. The PSNR, RelErr and SSIM values for $L = 33$ and $L = 10$ are reported in Table 1. Throughout the paper, *Iter* denotes the maximum number of iterations. It is clear that our method also behaves slightly better than the AA method.

The third simulated test data is the "House" image. In Table 1, we report the performance of the proposed method and the AA method for the speckled "House" in Figure 6 with $L = 25$ and $L = 3$, respectively. The restoration results are shown in Figure 6. From Figure 7, it is obvious that the SSIM maps of the restored images obtained by our method are much whiter than those by the AA method. Also, in Table 1, we observe that the PSNR and SSIM values are higher using our method.

In the fourth test, we deal with a more complicated case, that is, the original image is also blurred. The original image "Lena" has been blurred by a 5-by-5 average kernel,

https://doi.org/10.1017/S1446181114000339 Published online by Cambridge University Press

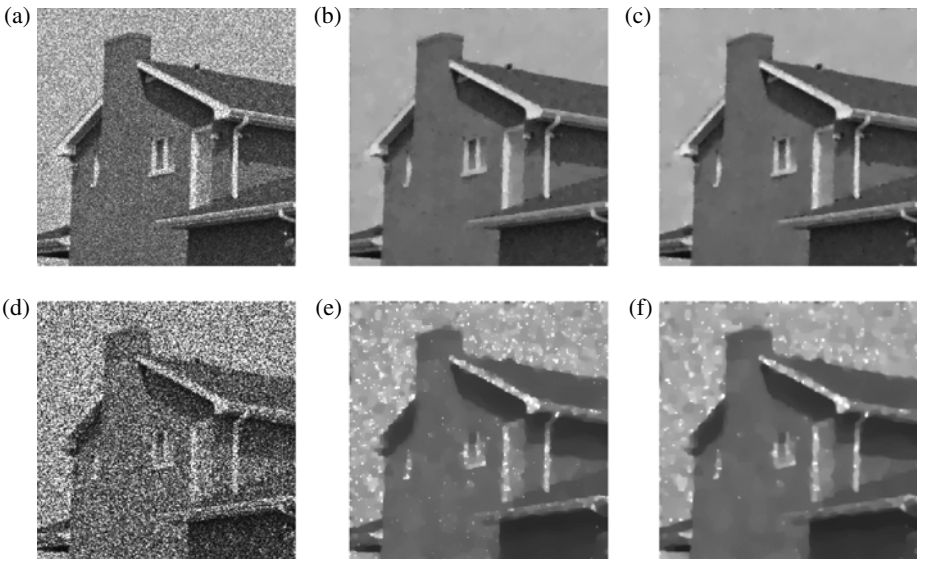

FIGURE 6. Results of different methods for removing multiplicative noise (House). (a) and (d) are the noisy images corrupted by multiplicative noise with $L = 25$ and $L = 3$, respectively; (b) and (e) the restored images by the AA method; (c) and (f) the restored images by the proposed method.

and then corrupted by a gamma noise with $L = 10$. In this case, the blurred matrix, K, is generated by the function *PsfMatrix* [30]. We use the periodic boundary conditions so that the blurred matrix K has a circulant with block structure. The blurred and noisy image is shown in Figure 8(a). From Figures 8(c) and (d), we see that the restored images obtained by our method have more detail than those by the AA method. In Figures 8(e) and (f), we zoom in on parts of the recovered images (shown as the white rectangle in Figure 8(a)). The comparison of SSIM maps shown in Figures 8(g) and (h) also proves that our method gives a better result. We report the PSNR, RelErr, and SSIM values in Table 3, which shows that our method behaves much better.

From the above experiments, we observe that our method obtains much better results than the AA method, and our method can alleviate the staircase effects efficiently. And from numerical results in terms of PSNR, RelErr, and SSIM reported in Table 1, our method yields a better restoration result. We also display the parameters chosen for the AA method and our method in Tables 2 and 3.

In the fifth test, we use a synthetic image of size 256×256 to show the power of reduction of the staircase effects with our method. The original image in Figure 9(a) is corrupted by gamma noise with $L = 25$. The noisy image is displayed in Figure 9(b). The restored images produced by the AA method and our method are shown in Figures 9(c) and (d), respectively. In this test, the highest PSNR value for the AA method is achieved for $\lambda = 550$ while the highest one for the proposed method is achieved for $\lambda = 500$. Without zooming in, staircasing is can already be detected in the AA method. We present the SSIM maps of the restored images in

https://doi.org/10.1017/S1446181114000339 Published online by Cambridge University Press

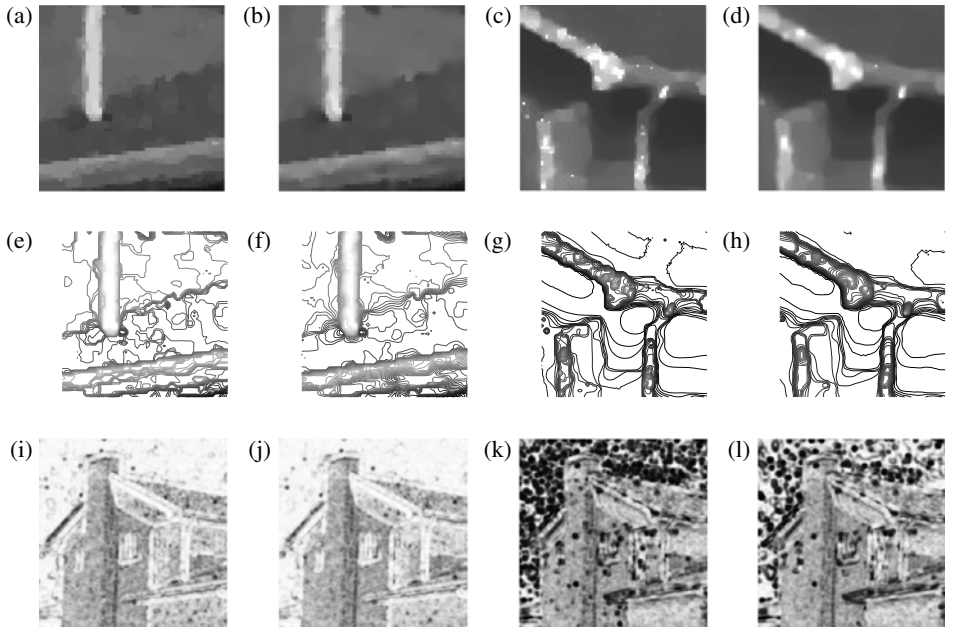

FIGURE 7. The small portions and the SSIM maps of the restored images (House). (a)–(d) The small portions of the restored images are shown for better visualization of the results: (a) and (b) are small parts of the restored images with $L = 25$; (c) and (d) are small parts of the restored images with $L = 3$. (e)–(h) The contours of the small parts: (e) and (f) are contours with $L = 25$; (g) and (h) are contours with $L = 3$. (i)–(l) The SSIM maps of the restored images: (i) and (j) are SSIM maps with $L = 25$; (k) and (l) are SSIM maps with $L = 3$.

TABLE 1. Numerical results for the denoising examples.

Images	Methods	PSNR	RelErr	SSIM	PSNR	RelErr	SSIM
		$L = 15$ #Iter = 500			$L = 5$ #Iter = 900		
Cameraman	AA	26.75	0.0874	0.79	23.72	0.1238	0.73
	Ours	26.95	0.0854	0.80	23.87	0.1216	0.74
		$L = 33$ #Iter = 500			$L = 10$ #Iter = 700		
Lena	AA	28.95	0.0684	0.84	25.88	0.0973	0.77
	Ours	29.25	0.0661	0.85	26.06	0.0954	0.78
		$L = 25$ #Iter = 500			$L = 3$ #Iter = 700		
House	AA	29.77	0.0569	0.82	22.11	0.1374	0.57
	Ours	30.08	0.0549	0.83	23.11	0.1224	0.64

Figures 9(e) and (f). We see from Figures 9(e) and (f) that the SSIM map of the restored image by the proposed method is whiter than that by the AA method, that is, our method can get better restoration results. In order to show the convergences of the AA method and our method, we give a plot about the relative error versus iterations

https://doi.org/10.1017/S1446181114000339 Published online by Cambridge University Press

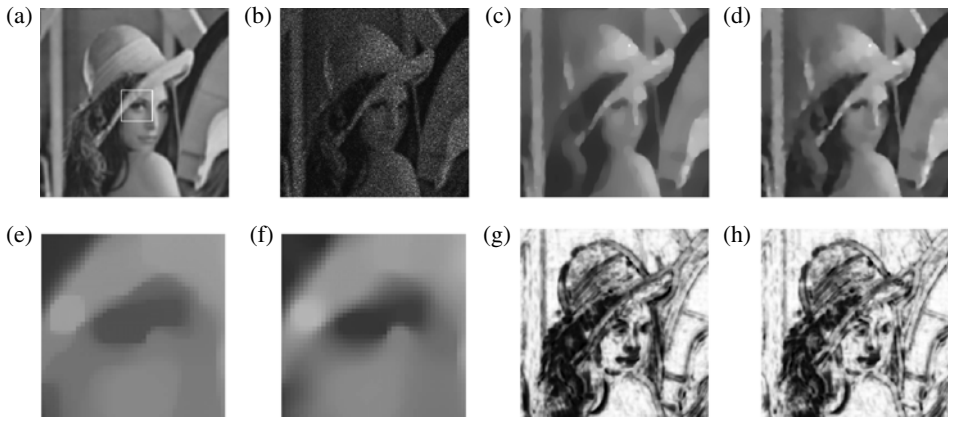

FIGURE 8. Restoration of blurred images corrupted by multiplicative noise: (a) the original image blurred by 5-by-5 average blur kernel; (b) the blurred and noisy image with $L = 10$; (c) and (d) restored results by the AA method and our method, respectively; (e) and (f) the zoomed-in parts of the restored results; (g) and (h) SSIM maps of the corresponding restored results.

TABLE 2. The parameters λ and the CPU time in seconds by different methods for the denoising examples.

Images	Methods	λ	Time(s)	λ	Time(s)
		$L = 15$ #Iter = 500		$L = 5$ #Iter = 900	
Cameraman	AA	570	11.78	110	19.87
	Ours	640	31.82	120	54.60
		$L = 33$ #Iter = 500		$L = 10$ #Iter = 700	
Lena	AA	1000	11.78	350	17.96
	Ours	1300	30.67	400	46.50
		$L = 25$ #Iter = 500		$L = 3$ #Iter = 700	
House	AA	700	10.90	0.5	15.04
	Ours	750	30.75	20	42.04

TABLE 3. Numerical results for the deblurring example (the parameters λ and the CPU time in seconds by different methods).

Image	Methods	PSNR	RelErr	SSIM	λ	Time(s)
		$L = 10$ #Iter = 700				
Lena	AA	22.20	0.1488	0.63	15	23.67
	Ours	23.74	0.1247	0.68	300	53.34

in Figure 9(g). For better visualization, zoom-ins of the same regions are shown in Figures 9(h) and (i). We see from Figure 9(i) that the staircase effects have been successfully alleviated in the proposed method. We give the contours of the zoomed-in parts in Figures 9(j) and (k), from which we reach similar conclusions.

https://doi.org/10.1017/S1446181114000339 Published online by Cambridge University Press

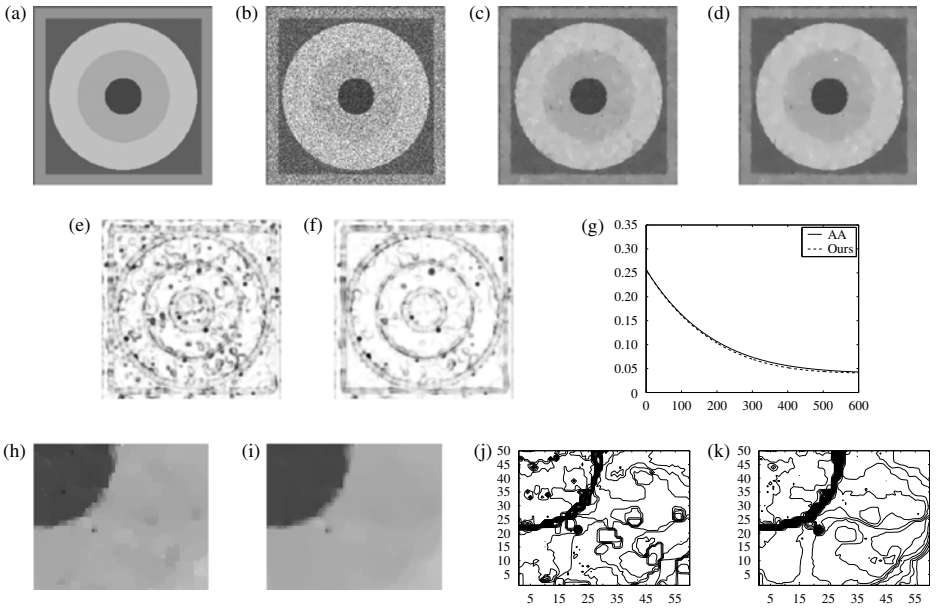

FIGURE 9. Results of different methods for a synthetic image: (a) original image; (b) noisy image with $L = 25$; (c) restored image by the AA method; (d) restored image by our method; (e) and (f) SSIM maps of restored images by the AA method and our method, respectively; (g) relative error versus iterations; (h) and (i) zoomed-in parts of the restored results; (j) and (k) contours of the zoomed-in parts.

Finally, to show the better ability of our method, we present nonspeckled images of various real SAR images in Figures 10(a)–(d). Since we do not have the reference images, the comparison between the AA method and the proposed method is not carried out here. In Figures 10(e)–(h) we display the restoration results obtained by the proposed method. From these figures, it is easy to see that the proposed method is very efficient for multiplicative noise removal.

5. Conclusion

We have analysed the variational method for the multiplicative noise removal problem. Based on a good feature of a high-order functional, we propose a model by adding an extra high-order functional term in the AA model. The numerical results show that the proposed method outperforms the AA method in terms of the PSNRs, relative errors and SSIM values. A comparison between the reconstructed images obtained by the two methods shows that the proposed one can alleviate the staircase effects significantly, while preserving edges. Since our proposed model is nonconvex, we employ the time-marching method to solve the minimization problem. Therefore, we can only achieve its local minimizer. Further research will focus on studying a strictly convex objective function for the multiplicative noise removal problem and using the alternating direction method of multipliers (ADMM) algorithm to solve it.

https://doi.org/10.1017/S1446181114000339 Published online by Cambridge University Press

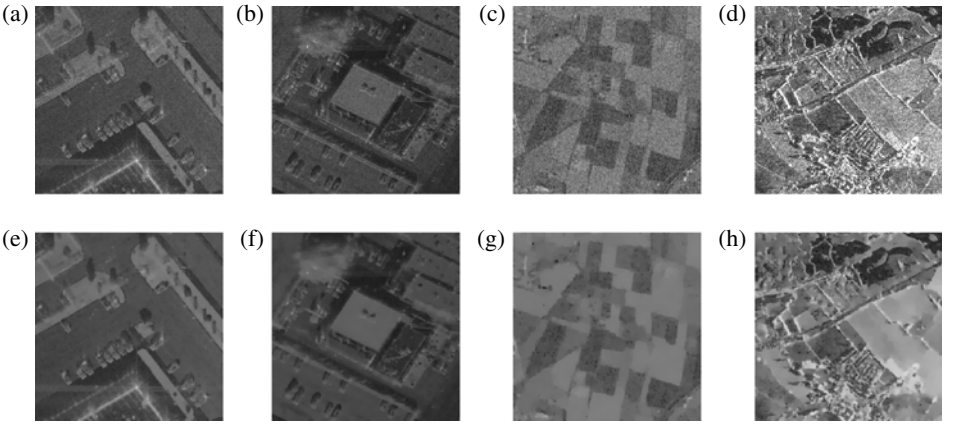

FIGURE 10. Nonspeckled images obtained by our method: (a) SAR image with size 391×391; (b) SAR image with size 391×391; (c) SAR image with size 256×256; (d) SAR image with size 256×256; (e)–(h) restoration results.

Acknowledgements

The authors would like to thank the referees for much constructive, detailed and helpful advice regarding revising this manuscript. This research is supported by NSFC (61401172, 61170311), Sichuan Province Sci. and Tech. Research Project (2012GZX0080), Nature Science Foundation of Jiangsu Province (BK20131209), and Postdoctoral Research Funds (2013M540454, 1301064B).

Appendix

PROOF OF THEOREM 2.3. Let $\alpha = \inf_\Omega g$ and $\beta = \sup_\Omega g$, and $u_n \in BV(\Omega) \cap BV^2(\Omega)$ be a minimizing sequence for the problem (2.2). We remark that $\log u + g/u$ is decreasing if $u \in (0, g)$, and strictly increasing for $u \in (g, \infty)$. Hence, we can always have

$$\int_\Omega \left(\log \sup(u, \alpha) + \frac{g}{\sup(u, \alpha)}\right) dx\, dy \le \int_\Omega \left(\log u + \frac{g}{u}\right) dx\, dy.$$

Moreover,

$$\int_\Omega |\nabla(\sup(u, \alpha))|\, dx\, dy \le \int_\Omega |\nabla u|\, dx\, dy$$

and

$$\int_\Omega |\nabla^2(\sup(u, \alpha))|\, dx\, dy \le \int_\Omega |\nabla^2 u|\, dx\, dy,$$

which can be derived similarly, as in Lemma 1 [21, Section 4.3]. Then we get

$$E(\sup(u, \alpha)) \le E(u),$$

and also $E(\inf(u, \beta)) \le E(u)$ in the same way. Therefore, we can assume without restriction that $\alpha \le u_n \le \beta$, which implies that u_n is bounded in $L_1(\Omega)$.

https://doi.org/10.1017/S1446181114000339 Published online by Cambridge University Press

By the definition of $\{u_n\}$, there exists a constant c such that $E(u_n) \le c$. Since $\int_\Omega (\log u + g/u)\,dx\,dy$ reaches its minimum value, $\int_\Omega (1 + \log g)\,dx\,dy$, when $u = g$, we can deduce that $\int_\Omega |\nabla u|\,dx\,dy$ and $\int_\Omega |\nabla^2 u|\,dx\,dy$ are bounded.

Thus, u_n is bounded in $BV(\Omega) \cap BV^2(\Omega)$, and there exists u in $BV(\Omega) \cap BV^2(\Omega)$ such that $u_n \to u$ in $BV(\Omega) \cap BV^2(\Omega)$ weak* and $u_n \to u^*$ in $L_1(\Omega)$ strong. According to the lower semicontinuity of $\int_\Omega |\nabla u|\,dx\,dy$ and $\int_\Omega |\nabla^2 u|\,dx\,dy$, $\alpha \le u^* \le \beta$ and *Fatou's lemma* [13], we get u^* as a solution to the problem (2.2). This completes the proof of Theorem 2.3. □

References

[1] H. C. Andrew and B. R. Hunt, *Digital image restoration* (Prentice Hall, Englewood Cliffs, NJ, 1977).

[2] G. Aubert and J. F. Aujol, "A variational approach to remove multiplicative noise", *SIAM J. Appl. Math.* **68** (2008) 925–946; doi:10.1137/060671814.

[3] M. R. Banham and A. K. Kataggelos, "Digital image restoration", *IEEE Signal Processing Mag.* **14**(2) (1997) 24–41; doi:10.1109/79.581363.

[4] M. Bertero and P. Boccacci, *Introduction to inverse problems in imaging* (Institute of Physics Publishing, London, 1998); doi:10.1887/0750304359.

[5] J. M. Bioucas-Dias and M. A. T. Figueiredo, "Multiplicative noise removal using variable splitting and constrained optimization", *IEEE Trans. Image Process.* **19**(7) (2010) 1720–1730; doi:10.1109/TIP.2010.2045029.

[6] A. Buades, B. Coll and J. M. Morel, "A review of image denoising algorithms, with a new one", *SIAM Multiscale Model. Simul.* **4** (2005) 490–530; doi:10.1137/040616024.

[7] A. Chambolle, "An algorithm for total variation minimization and applications", *J. Math. Imaging Vision* **20** (2004) 89–97; doi:10.1023/B:JMIV.0000011325.36760.1e.

[8] T. F. Chan, A. Marquina and P. Mulet, "High-order total variation-based image restoration", *SIAM J. Sci. Comput.* **22** (2000) 503–516; doi:10.1137/S1064827598344169.

[9] T. F. Chan and J. H. Shen, *Image processing and analysis: variational, PDE, wavelet, and stochastic methods* (SIAM, Philadelphia, 2005); doi:10.1137/1.9780898717877.

[10] D. Q. Chen and L. Z. Cheng, "Spatially adapted total variation model to remove multiplicative noise", *IEEE Trans. Image Process* **21** (2007) 1650–1662; doi:10.1109/TIP.2011.2172801.

[11] H. Z. Chen, J. P. Song and X. C. Tai, "A dual algorithm for minimization of the LLT model", *Adv. Comput. Math.* **31** (2009) 115–130; doi:10.1007/s10444-008-9097-0.

[12] T. R. Crimmins, "Geometric filter for reducing speckle", *Opt. Eng.* **25** (1986) 651–654; doi:10.1117/12.949543.

[13] E. A. Feinberg, P. O. Kasyanov and N. V. Zadoianchuk, 'Fatou's lemma for weakly converging probabilities', Preprint, 2012, arXiv:1206.4073.

[14] C. Fox, *An introduction to the calculus of variations* (Dover Publications, New York, 1987).

[15] T. Goldstein and S. Osher, "The split Bregman method for L1-regularized problems", *SIAM J. Imaging Sci.* **2** (2009) 323–343; doi:10.1137/080725891.

[16] J. Goodman, *Speckle phenomena in optics: theory and applications* (Roberts & Company Publications, Greenwood Village, CO, 2007).

[17] P. J. Green, "Reversible jump MCMC computation and Bayesian model, determination", *Biometrika* **82** (1995) 711–732.

[18] P. C. Hansen, J. G. Nagy and D. P. O'Leary, *Deblurring images: matrices, spectra, and filtering* (SIAM, Philadelphia, 2006); doi:10.1137/1.9780898718874.

[19] G. T. Herman, *Fundamentals of computerized tomography: image reconstruction from projections*, 2nd edn (Springer, New York, 2009); doi:10.1007/978-1-84628-723-7.

[20] Y. M. Huang, M. K. Ng and Y. W. Wen, "A new total variation method for multiplicative noise removal", *SIAM J. Imag. Sci.* **2** (2009) 20–40; doi:10.1137/080712593.

[21] P. Kornprobst, R. Deriche and G. Aubert, "Image sequence analysis via partial differential equations", *J. Math. Imaging Vision* **11** (1999) 5–26; doi:10.1007/s11263-005-4882-4.
[22] K. Krissian, C. F. Westin, R. Kikinis and K. G. Vosburgh, "Oriented speckle reducing anisotropic diffusion", *IEEE Trans. Image Process.* **16** (2007) 1412–1424; doi:10.1109/TIP.2007.891803.
[23] N. D. Laobeul, 'Regularization methods for ill-posed Poisson imaging problems', Ph.D. Thesis, University of Montana, 2008.
[24] P. M. Lee, *Bayesian statistics: an introduction* (Oxford University Press, New York, 1989).
[25] F. Li, M. Ng and C. M. Shen, "Multiplicative noise removal with spatial-varying regularization parameters", *SIAM J. Imaging Sci.* **3** (2010) 1–20; doi:10.1137/090748421.
[26] F. Li, C. M. Shen, J. S. Fan and C. L. Shen, "Image restoration combining a total variational filter and a fourth-order filter", *J. Vis. Commun. Image Representation* **18** (2007) 322–330; doi:10.1016/j.jvcir.2007.04.005.
[27] M. Lysaker, A. Lundervold and X. C. Tai, "Noise removal using fourth-order partial differential equation with applications to medical magnetic resonance images in space and time", *IEEE Trans. Image Process.* **12** (2003) 1579–1590; doi:10.1109/TIP.2003.819229.
[28] M. Lysaker and X. C. Tai, "Iterative image restoration combining total varition minimization and a second-order functional", *Int. J. Comput. Vision* **66** (2006) 5–18; doi:10.1007/s11263-005-3219-7.
[29] A. Marquina and S. Osher, "Explicit algorithms for a new time dependent model based on level set motion for nonliear deblurring and noise removal", *SIAM J Sci. Comput.* **22**(2) (2000) 387–405; doi:10.1137/S1064827599351751.
[30] J. G. Nagy, K. Palmer and L. Perrone, "Iterative methods for image deblurring: a Matlab object-oriented approach", *Numer. Algorithms* **36** (2004) 73–93; doi:10.1023/B:NUMA.0000027762.08431.64.
[31] A. W. Naylor and G. R. Sell, *Linear operator theory in engineering and science* (Springer, Berlin, 1982); doi:10.1007/978-1-4612-5773-8.
[32] C. Oliver and S. Quegan, *Understanding synthetic aperture radar images* (SciTech Publishing, Raleigh, NC, 2004).
[33] K. Papafitsoros and C. B. Schönlieb, "A combined first and second order variational approach for image reconstruction", *J. Math. Imaging Vision* **48** (2014) 308–338; doi:10.1007/s10851-013-0445-4.
[34] K. F. Riley, M. P. Hobson and S. J. Bence, *Mathematical methods for physics and engineering* (Cambridge University Press, Cambridge, 2006); doi:10.1017/CBO9780511810763.
[35] L. Rudin, P. L. Lions and S. Osher, "Multiplicative denoising and deblurring: theory and algorithms", in: *Geometric level sets in imaging, vision and graphics* (eds S. Osher and N. Paragios), (Springer, New York, 2003) 103–119; doi:10.1007/0-387-21810-6_6.
[36] L. Rudin, S. Osher and E. Fatemi, "Nonlinear total variation based noise removal algorithms", *Physica* D **60** (1992) 259–268; doi:10.1016/0167-2789(92)90242-F.
[37] J. Shi and S. Osher, "A nonlinear inverse scale space method for a convex multiplicative noise model", *SIAM J. Imag. Sci.* **1** (2008) 294–321; doi:10.1137/070689954.
[38] G. Steidl, "A note on the dual treatment of higher order regularization functionals", *Computing* **76** (2005) 135–148; doi:10.1007/s00607-005-0129-z.
[39] G. Steidl and T. Teuber, "Removing multiplicative noise by Douglas-Rachford splitting methods", *J. Math. Imaging Vision* **36** (2010) 168–184; doi:10.1007/s10851-009-0179-5.
[40] R. F. Wagner, S. W. Smith and J. M. Sandrik, "Statistics of speckle in ultrasound B-scans", *IEEE Trans. Sonics Ultrason* **30** (1983) 156–163; doi:10.1109/T-SU.1983.31404.
[41] Z. Wang, A. C. Bovik, H. R. Sheikh and E. P. Simoncelli, "Image quality assessment: from error visibility to structural similarity", *IEEE Trans. Image Process.* **13**(4) (2004) 600–612; doi:10.1109/TIP.2003.819861.
[42] Y. Wu and H. Maitre, "Smoothing speckled synthetic aperture radar images by using maximum homogeneous region filters", *Opt. Eng.* **31** (1992) 1785–1792; doi:10.1117/12.59897.
[43] Y. Yu and S. T. Acton, "Speckle reducing anisotropic diffusion", *IEEE Trans. Image Process.* **11** (2002) 1260–1270; doi:10.1109/TIP.2002.804276.